IET Science, Measurement & Technology

Research Article

IET Journals
The Institution of Engineering and Technology

Sensitivity-based optimal shape design of induction-heating devices

ISSN 1751-8822
Received on 25th July 2014
Accepted on 7th November 2014
doi: 10.1049/iet-smt.2014.0227
www.ietdl.org

Paolo Di Barba[1], Fabrizio Dughiero[2], Michele Forzan[2], Elisabetta Sieni[2] ✉

[1]*Department of Electrical, Computer and Biomedical Engineering, University of Pavia, Via Ferrata, 1, 27100 Pavia, Italy*
[2]*Department of Industrial Engineering, University of Padova, Via Gradenigo 6/A, 35131 Padova, Italy*
✉ *E-mail: elisabetta.sieni@unipd.it*

Abstract: A design of experiment (DOE) strategy applied to multi-objective optimisation is proposed in order to evaluate the influence of design variables variations to optimised quantities. A secondary objective function is the sensitivity of a primary objective function to design variable variations evaluated by means of DOE strategy. The optimisation problem includes also a third objective function that considers device constraint because of technological limitations on power generator. The proposed case study deals with the design of an electromagnetic device that will be used to carry out laboratory experiments on magneto-fluid hyperthermia, that is, a clinic treatment for cancer cure. The induction system is designed to apply a controlled time-varying magnetic field to biological cells, cultured in Petri dish and mixed with magnetic nanoparticles. This study presents an original cost-effective method of multi-objective design optimisation taking into account design uncertainties.

1 Introduction

Currently, the optimal design of electromagnetic device is largely researched also to include the effect of uncertainties on design variables or parameters [1–7]. In fact, in production process, the device and its components are affected by tolerances that can significantly modify its performance [8–12] and tolerance intervals are given to each geometrical dimension. The design of a device needs to find optimal solutions insensitive to small perturbations of design variables. Various strategies to take into account uncertain variables in the design of a device have been proposed, see, for example, [1–6, 11–14]; a comparative review of optimisation procedures based on worst-case scenario can be found in [2], whereas an approach based on the approximated Lipschitz constant is proposed in [15]. Another possible strategy is the concept of multidimensional hypercube centred on the current solution [16]. More generally, parametric and non-parametric multi-objective optimisation can be used in the design of electromagnetic devices [17–27].

The aim of the proposed multi-objective optimisation is to design an inductor to obtain homogenous magnetic field intensity in the bottom of a Petri dish used in some experiments of magneto-fluid hyperthermia [28–31]. In particular, the aim is to obtain a uniform magnetic field in a prescribed region to heat a magnetic nanoparticle fluid by means of a time-varying magnetic field at radio-frequency in the range of 100–400 kHz [32, 33]. Accordingly, the main objective function is the field inhomogeneity, to be minimised with respect to the geometric variables of induction-heating device; in this paper, the geometric model depends on five design variables. The second objective function is the sensitivity of the solution against small perturbations in a subset of three design variables, to be minimised too. Perturbations of design variables have been investigated using design of experiment (DOE) strategy [34, 35]. Finally, a third objective function is defined in terms of either the voltage at inductor ends or the supplied electrical current. Therefore an optimal shape-design problem characterised by three-objective space is investigated. A detailed description of the case study is given in Section 3.

In the past, the DOE strategy has been proposed, for example, in [34] to numerically evaluate the sensitivity of a solution with respect to a small perturbation of some parameters not incorporated in the design variable set, like material properties in a problem of optimal shape design. In this paper, in turn, the DOE strategy has been applied to evaluate the sensitivity of a solution just with respect to variations of design variables in a cost-effective way; moreover, sensitivity is considered as an additional objective function. Methodological aspects are focused on in Section 2.

2 Sensitivity computation methods

The sensitivity of design variables was computed using a DOE strategy [34] in order to evaluate the effect of a set of uncertain parameters meant as quantities different from the design variables. In contrast, the same DOE strategy is here applied to a subset of N_p out of N design variables, $N_p < N$ (N is the total number of design variables, N_p is the number of uncertain design variables in the subset).

2.1 DOE method

According to the multi-factorial DOE strategy [35] in the case of $N_p = 3$, given the current solution of the optimisation problem, four extra solutions (Y_j, $j = 1, 4$) are computed by varying the values of the uncertain variables, p_k $k = 1, \ldots, 3$, around their current nominal value, as shown in Table 1. To consider more than three uncertain variables, according to the DOE strategy proposed by Placket–Burmann [35], a table of sign alternance with more experiments has to be considered. Sign alternance follows the Placket–Burmann rule [35]. For instance, when the uncertain variables are between 4 and 7, 8 supplementary experiments, $k = 1, \ldots, 8$, are required. In Table 1, it is assumed that the N_p uncertain design variables has been attributed an uncertainty range; then the signs '+' and '−', in Table 1, correspond to select the upper or lower limit in the range of the design variable uncertainty, respectively.

Therefore, given a solution, four values of the f_i objective functions, named $f_{i,j}$, $j = 1, \ldots, 4$, ($f_{i,1}$, $f_{i,2}$, $f_{i,3}$, $f_{i,4}$), are computed by varying the design variable values as described as follows. Given the step function defined as

$$U(Y_j, p_k) = \begin{cases} 1, & \text{if } (Y_j, p_k) = '+' \\ 0, & \text{if } (Y_j, p_k) = '-' \end{cases} \quad (1)$$

Table 1 Table of design: sign alternance of uncertain variables p_k, $k = 1, 3$ for evaluating sensitivity

	p_1	p_2	p_3	f_i ($i = 1$)
Y_1	+	+	+	$f_{i,1}$
Y_2	−	+	−	$f_{i,2}$
Y_3	−	−	+	$f_{i,3}$
Y_4	+	−	−	$f_{i,4}$

the sensitivity is evaluated this way [34]: for the kth uncertain design variable, $k = 1, 3$, the sums of f_i values ($f_{i,j}$) corresponding to a '+' in Table 1, $S_{+,Pk}$, and the ones corresponding to a '−', $S_{-,Pk}$, are computed as follows

$$S_{+,Pk} = \sum_{j=1}^{4} f_{i,j} \cdot U(Y_j, p_k) \tag{2}$$

$$S_{-,Pk} = \sum_{j=1}^{4} f_{i,j} \cdot \left[1 - U(Y_j, p_k)\right] \tag{3}$$

Then, the influence s_{Pk} of a variation of the kth design variable on the value of objective function f_i is evaluated as [34]

$$s_{Pk} = \frac{S_{+,Pk}}{N_+} - \frac{S_{-,Pk}}{N_-} \tag{4}$$

where N_+ and N_- are the number of sign '+' and '−' in the column corresponding to the considered variable in Table 1. For the kth design variable, the partial sensitivity, s_{Pk}, is estimated just using (4), which is the core equation. After (4) it can be remarked that the multi-factorial DOE (linear number of experiments) is cost-effective with respect to the full-factorial DOE (exponential number of experiments). Finally, the total sensitivity with respect to all the uncertain design variable, f_2, is given by

$$f_2 = \sqrt{\sum_{k=1}^{3} s_{Pk}^2} \tag{5}$$

Under a multi-objective context, f_2 given by (5) can well be regarded as a secondary objective function in addition to the design criterion f_1: this is exactly the leading idea of Section 3.

2.2 Method comparison and validation

For the sake of a comparison, the sensitivity of f_1 is computed also by means of a different method, that is, using Taylor first-order approximation and varying only one design variable at a time inside the interval $\pm d$, for example, $d = 1$ mm

$$\frac{\partial f_1}{\partial x_i} \cong \frac{f_1(x_i + d) - f_1(x_i - d)}{2d} \quad \left[\frac{\text{points}}{\text{mm}}\right] \tag{6}$$

Given the uncertainty σ_k in [millimetres] computed for the kth design variable, and given the objective function f_1, computed for the current solution and evaluated in [points], the global effect of a variation of a design variable on the solution S_n, $\sigma_{i,n}(S_n)$, is calculated using a classical method to evaluate measurement uncertainty [36]

$$\sigma_{i,n}(S_n) = \sqrt{\sum_{k=1}^{N_p} \left(\frac{\partial f_i}{\partial x_k}\right)^2 \sigma_k^2} \quad [\text{points}] \tag{7}$$

Equation (7) is a more accurate method to evaluate the influence of a variation of a set of N_p variables on function f_i. In fact, (7) includes the weight of a variation of each variable (with a value <1 or >1) evaluated as a derivative of the examined objective function. In this paper, the derivative is approximated numerically performing two extra simulations for each design variables around the solution evaluated by means of the optimisation procedure. It is expected that (5), that is, an estimation of the solution variability, be comparable with (7).

3 Case study

In Fig. 1*a*, the cross-section of the axi-symmetric geometry of the device considered as the case study is shown [37]. The electromagnetic device is composed of an inductor with two copper turns, four ferrite rings and a ferrite disc placed as in Fig. 1*a*. Ferrite blocks allow to shape the magnetic flux lines in

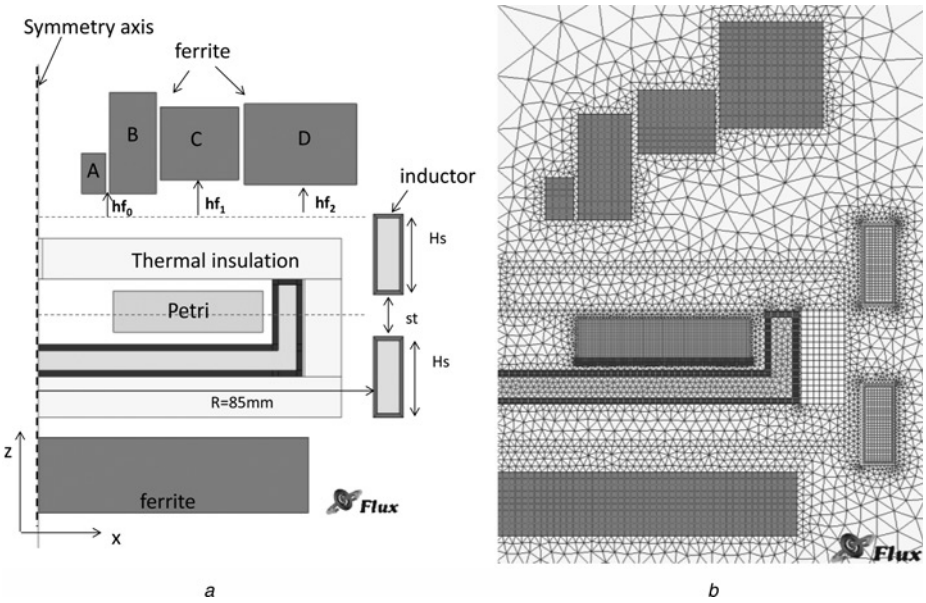

Fig. 1 *Case study*

a Geometry of the induction-heating device with design variables (the uncertain ones are in bold character)
b Detail of the FE mesh

IET Sci. Meas. Technol., 2015, Vol. 9, Iss. 5, pp. 579–586

Table 2 Lower and upper bounds of design variables and uncertainty intervals of design variables

Uncertain design variable	Range, mm	Uncertainty, mm	Design variable	Range, mm
hf_0	[1, 30]	±1	H_S	[10, 60]
hf_1	[1, 30]	±1	st	[0, 30]
hf_2	[1, 30]	±1		

order to achieve the prescribed field homogeneity. The size of ferrite blocks has been chosen using some preliminary results presented in [37], and considering ferrite elements commercially available. A Petri dish is placed in a thermally insulated box in order to mitigate the influence of the environment temperature; in Fig. 1*a*, the thermal box is sketched only to show the whole device: in fact, temperature field simulation falls out of the scope of the work. The magnetic problem is solved in time-harmonics conditions using a finite element (FE) code [38]. The inductor can be supplied by imposing either a current (e.g. 500 A_{rms} at 350 kHz) or a voltage (600 V_{rms} at 350 kHz). A typical mesh (Fig. 1*b*) exhibits 24 000 nodes and 9900 second-order surface elements.

Table 2 shows the $N = 5$ design variables characterising the case study, with the relevant range; the uncertainty intervals of the N_p design variable subset (height of the ferrite disks in the upper part of the device, that is, hf_0, hf_1 and hf_2 in Fig. 1*a*) are also prescribed. The other two design variables are the z-directed size of the inductor turn, H_S, and the distance between the two inductor turns, st.

3.1 Electromagnetic analysis problem

The electromagnetic axi-symmmetric problem is solved using the $\boldsymbol{A}$–V formulation. The problem is solved in terms of the phasor of magnetic vector potential, $\boldsymbol{A}$, coupled with the electric scalar potential, V. When the Coulomb gauge is applied on the magnetic vector potential, that is, $\nabla \cdot \dot{\boldsymbol{A}} = 0$, the following coupled equations are solved [39]

$$\nabla \times \frac{1}{\mu} \nabla \times \dot{\boldsymbol{A}} + \mathrm{j}\omega\mu \frac{1}{\rho} \dot{\boldsymbol{A}} = -\frac{1}{\rho} \nabla \dot{V} \tag{8}$$

$$\nabla \cdot \frac{1}{\rho} (\mathrm{j}\omega\mu \dot{\boldsymbol{A}} + \nabla \dot{V}) = 0 \tag{9}$$

with μ being the material permeability, ω is the field pulsation and ρ is the material resistivity for copper turns, while $\dot{\boldsymbol{A}}$ is the phasor of the magnetic vector potential.

3.2 Optimisation problem

The optimisation aim is three-fold: maximising the magnetic field homogeneity in the bottom of the Petri dish, minimising the design sensitivity and limiting the voltage supply at inductor ends or, alternatively, the inductor current. Consequently, the following three-objective functions have been considered:

(f_1) is the inhomogeneity of the magnetic field, H, on the bottom of the Petri dish, to be minimised as in [37] with a tolerance interval of ±10 A/m. Once (8) and (9) are solved, the H-field intensity can be computed from magnetic vector potential $\boldsymbol{A}$ in a straight forward way. Therefore the inhomogeneity of H in terms of the H-norm discrepancy, that is dimensionless, is evaluated on the bottom of the Petri dish on a fixed grid of points;
(f_2) is the sensitivity of f_1 with respect to the set of uncertain design variables shown in Table 2, evaluated according to (5), to be minimised; and
(f_3) is the end voltage (or current) when the inductor is supplied by applying a current (or a voltage, respectively). The rationale is that, in general, the end voltage must not exceed the typical value available at the converter output (e.g. 700 V_{rms} as maximum voltage of capacitance with a current up to 700 A_{rms}). The third objective function, f_3, can consider the following two cases:

(a) the inductor has been supplied by a current I of 500 A_{rms} at 350 kHz, and the voltage at the inductor ends (f_3) is minimised and
(b) alternatively, the inductor has been supplied by a voltage of 600 V_{rms} at 350 kHz, and the supply current (f_3) is minimised.

The aforementioned objective functions, subject to bounds in Table 2, have been minimised in the Pareto sense (i.e. search for the front of non-dominated solutions) using a standard evolutionary algorithm (Non-dominated Sorting Genetic Algorithm (NSGA)-II).

An additional remark on voltage and current calculation in the inductor is worthwhile. The FE electromagnetic solution takes into account the actual distribution of current density in the inductor, I_{turn}, that in turn depends on the induced electric field and the voltage applied by an external supply. The last quantity represents the imposed current source

$$\dot{I}_{turn} = -\frac{1}{\rho} \int_{S_{turn}} (\mathrm{j}\omega\mu \dot{\boldsymbol{A}} + \nabla \dot{V}) \, \mathrm{dS} \tag{10}$$

where S_{turn} is the cross-sectional area of the inductor turn, normal to the current flow in a 2D axi-symmetric model. The inductor is composed by two turns series connected, so each turn must carry the same current intensity. When the external supply imposes a current intensity, the applied voltage is calculated for each turn using a circuital approach based on the node-voltage analysis to fulfil the requirements about total imposed current and series connected turns. The same circuital approach is applied to compute the complex voltage values of each turn when the total voltage is the supply value (the solution is trivial when the inductor comprises only 2 turns). As a consequence, the value of voltage (or current) to feed the inductor depends on the actual electromagnetic field distribution that affects the induced term.

The implemented version of NSGA-II algorithm [15, 25, 34] exploits simulated binary cross-over (Simulated Binary Crossover (SBX) algorithm [40]) with a probability of cross-over of 0.9 and polynomial mutation, with a mutation probability of $1/N$. The distribution indices for cross-over and mutation operators are both equal to 20. The number of individual for each generation is 20 and the number of generations is 50. The optimisation process lasted approximately one day using a 64 bit workstation with 24 GB random access memory and an Intel Xeon central processing unit at 3.33 GHz. Results are presented in Section 4.

4 Results

The results of the two optimisation case studies defined in Section 3 are summarised. In case (a), the voltage at inductor ends is minimised, whereas in case (b) the current in the inductor is minimised.

4.1 Case (a)

Fig. 2 reports the approximated three-dimensional (3D) Pareto front that was obtained by minimising the three-objective functions in the case of the inductor supplied by a constant current. Each point in Fig. 2 corresponds to a different FE analysis. Black crosses represent the non-dominated solutions among all generated individuals.

Fig. 3 reports the corresponding 2D orthogonal projections of the 3D front: sensitivity (f_2) and inductor voltage (f_3) as a function of the magnetic field inhomogeneity (f_1).

In Table 3, a set of four solutions located along the Pareto fronts are reported in terms of design variables and objective functions values. The corresponding geometries are shown in Fig. 4.

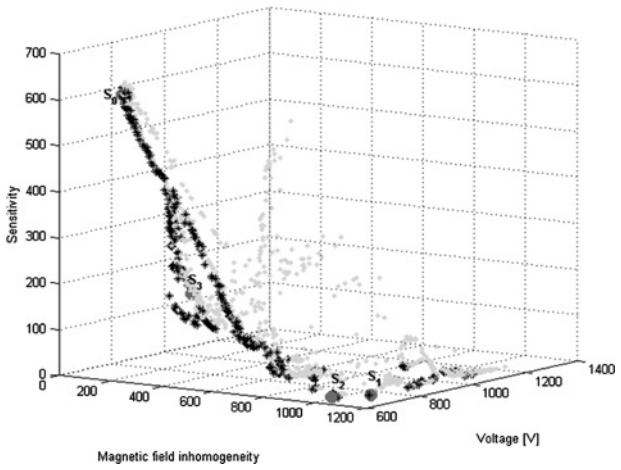

Fig. 2 *3D objective space: generated individuals (Grey points) and approximated Pareto front (black crosses)*

Solutions in Table 3 have been highlighted

Table 3 Selected solutions on the Pareto front

	hf_0, mm	hf_1, mm	hf_2, mm	H_s, mm	st, mm	f_1	f_2	f_3, V
S_0	8.02	17.16	7.54	60	8.52	188	614.9	656.3
S_1	1.93	14.76	29.39	42.19	28.84	1080	2.8	735
S_2	13.44	30	25.67	59.89	25.36	1048	12.9	616.5
S_3	20.45	19.82	21.33	49.72	3.79	376	182.6	737.8

Design variables, objective functions f_1, f_2 and f_3.

Fig. 5*a* reports the magnetic field intensity along a line in the bottom of the Petri dish. The magnetic flux lines and the magnetic field intensity on the Petri dish are shown in Fig. 5*b*. The typical value of magnetic field, in the examined case, is close to 7 kA/m (peak value).

The effects on objective functions because of a positive or negative variation of an uncertain design variable at a time (the ones used in the DOE computation) are reported in Table 4. For each solution, S_i, the optimised values are shown (row named 'Start'). The second row, named ('round'), shows the effect on objective functions because of rounding the design variable values to the nearest integer and, finally, the effect obtained by applying a perturbation to a single design variables in the set of N_p ones. Considering the objective function f_1, the partial derivatives (6) are computed for the design variable hf_0, hf_1 and hf_2. In particular, '$hf_{k,+}$' and '$hf_{k,-}$' correspond to a positive or negative variation of the design variable h_{fk}, $k = 1, 3$, respectively.

Finally, the sensitivity of each solution in Table 3, computed on design variables using (4) and data in Table 4, is reported in Table 5. To compute (4), four extra FE computations are needed. To compute (7) the extra FE solutions are six. To compare the two methods to evaluate the sensitivity of a solution, Table 5 reports also the values of the sensitivity computed by means of DOE strategy. The values of the sensitivity computed using (4) are proportional with the ones computed using the DOE strategy during the optimisation process (Fig. 6).

It appears that the better solution in terms of magnetic field uniformity is the more sensitive to design variables variations,

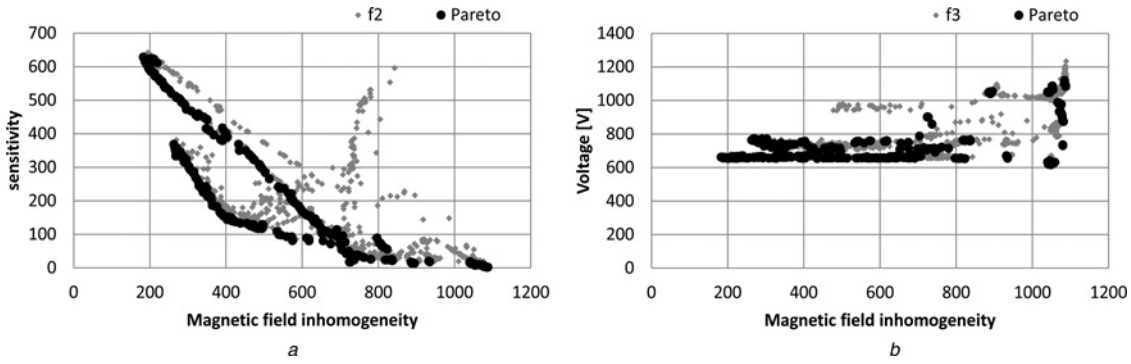

Fig. 3 *2D orthogonal projections of Pareto fronts*

a Sensitivity
b Voltage against H inhomogeneity

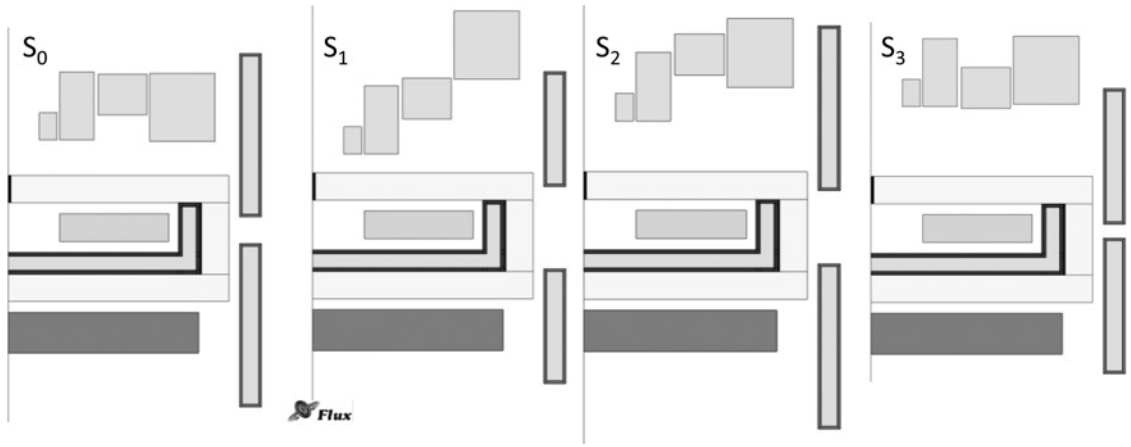

Fig. 4 *Geometries of the designed device for solutions on Pareto front for the case (a)*

IET Sci. Meas. Technol., 2015, Vol. 9, Iss. 5, pp. 579–586

Table 4 Effect of a variation $d = \pm 1$ mm on the solutions listed in Table 3

		hf_0, mm	hf_1, mm	hf_2, mm	H_s, mm	st, mm	f_1	f_2	f_3, V
S_0	start	8.02	17.16	7.54	60	8.52	188	616.4	656.3
	round	8	17	8	60	9	274	572	654.8
	$hf_{0,+}$	9	17	8	60	9	529	250.9	654.4
	$hf_{0,-}$	7	17	8	60	9	805	316.3	655.3
	$hf_{1,+}$	8	18	8	60	9	263	584	655.1
	$hf_{1,-}$	8	16	8	60	9	284	556.9	654.7
	$hf_{2,+}$	8	17	9	60	9	775	309.3	655.2
	$hf_{2,-}$	8	17	7	60	9	532	262.7	654.6
S_1	start	1.93	14.76	29.39	42.19	28.84	1080	2.8	735.1
	round	2	15	29	42	29	1080	2.2	737.4
	$hf_{0,+}$	3	15	29	42	29	1080	5.5	735.9
	$hf_{0,-}$	1	15	29	42	29	1081	3.3	738.9
	$hf_{1,+}$	2	16	29	42	29	1081	2.2	738.7
	$hf_{1,-}$	2	14	29	42	29	1080	5.1	735.3
	$hf_{2,+}$	2	15	30	42	29	1080	4.6	734.5
	$hf_{2,-}$	2	15	28	42	29	1080	2.2	739.4
S_2	start	13.44	30	25.67	59.89	25.36	1048	12.9	616.5
	round	13	30	26	60	25	1051	12.1	617.3
	$hf_{0,+}$	14	30	26	60	25	1046	14.3	616.4
	$hf_{0,-}$	12	30	26	60	25	1056	10.4	618.1
	$hf_{1,+}$	13	31	26	60	25	1050	12.1	617.1
	$hf_{1,-}$	13	29	26	60	25	1052	10.7	617.4
	$hf_{2,+}$	13	30	27	60	25	1054	10.1	617.9
	$hf_{2,-}$	13	30	25	60	25	1047	13.6	616.7
S_3	start	20.45	19.82	21.33	49.72	3.79	376	182	737.8
	round	20	20	21	50	4	382	182.2	735.4
	$hf_{0,+}$	21	20	21	50	4	427	151.5	735.1
	$hf_{0,-}$	19	20	21	50	4	474	202	735.9
	$hf_{1,+}$	20	21	21	50	4	364	219.1	734.6
	$hf_{1,-}$	20	19	21	50	4	400	159.7	736.5
	$hf_{2,+}$	20	20	22	50	4	463	151.3	734.7
	$hf_{2,-}$	20	20	20	50	4	412	170.5	736.2

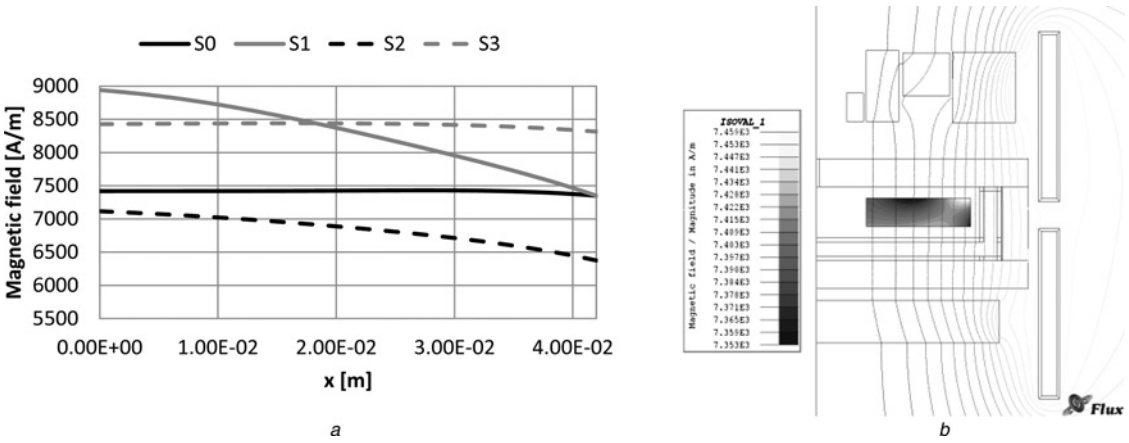

Fig. 5 *Magnetic field intensity along a line in the bottom of the Petri dish*

a Magnetic field in the bottom of the Petri dish as a function of the x-coordinate
b Magnetic flux line of direct problem and magnetic field colour map on the Petri dish for solution S_0

whereas the worst case in terms of homogeneity is the less sensitive.

4.2 Case (b)

Fig. 7 reports the 3D Pareto front obtained minimising the three-objective functions for the inductor supplied by a constant

Table 5 Approximated partial derivatives computed using (6) and sensitivity, for solutions in Table 3, exploiting (5), (7) and Table 4

	$\partial f_1/\partial(hf_0)$	$\partial f_1/\partial(hf_1)$	$\partial f_1/\partial(hf_2)$	$\sigma_{i,n}(S_n)$ (7)	f_2 (5)
S_0	−138	−10.5	121.5	212.7	614.9
S_1	−0.5	0.5	0	0.8	2.8
S_2	−5	−1	3.5	7.1	12.9
S_3	−23.5	−18	25.5	45.1	182.6

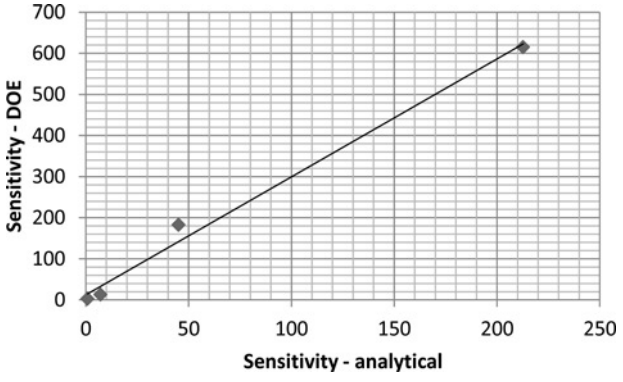

Fig. 6 *Sensitivity – DOE computed using (5) as a function of sensitivity – analytical computed using (7) for the case (a)*

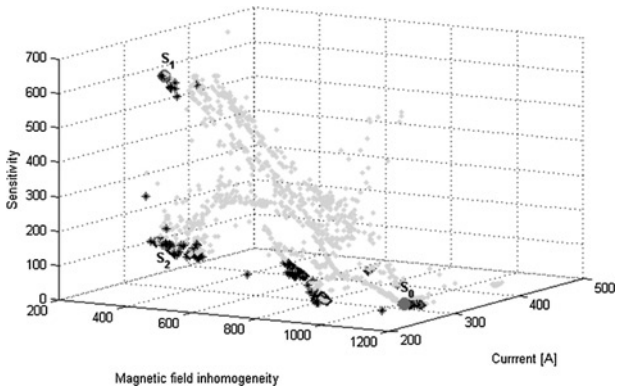

Fig. 7 *3D objective space: generated individuals (green points) and approximated Pareto front (black crosses)*

Solutions in Table 6 have been highlighted

voltage. Each point in Fig. 7 corresponds to a different FE analysis. Black crosses represent the non-dominated solutions among generated individuals.

Fig. 8 reports the corresponding 2D orthogonal projections of the 3D front: sensitivity (f_2) or current (f_3) as a function of the magnetic field inhomogeneity (f_1).

In Table 6, a set of three solutions on the Pareto front are reported in terms of design variables and objective functions values. The corresponding geometries are in Fig. 9.

Table 6 Selected solutions on the Pareto front

	hf_0, mm	hf_1, mm	hf_2, mm	H_s, mm	st, mm	f_1	f_2	f_3, A
S_0	1	20.7	26.7	19.8	17.2	1041	13	304.2
S_1	5.1	12.1	4.5	30.8	22	229	579.3	347
S_2	10.3	18.3	15.2	13.8	22.4	357	122.3	290.5

Design variables, objective functions f_1, f_2 and f_3.

Fig. 10*a* reports the magnetic field intensity along a line in the bottom of the Petri dish. The magnetic flux lines and the magnetic field intensity on the Petri dish are in Fig. 10*b*. In this case the typical value of magnetic field, in the examined case, is close to 6 kA/m (peak value); correspondingly, the current is close to 300 A.

In Table 7, the effects on objective functions of a positive or negative variation on a single design variable (only the ones used in the DOE computation) are reported. For each solution, S_i, the same evaluations reported in Table 4 have been repeated. Positive and negative variations on design variables as in case (a) have been applied.

Finally, the sensitivity of each solution in Table 6, computed on design variables using (4) and data in Table 7, is reported in Table 8. It can be underlined that the values of the sensitivity computed using (4) are proportional to the ones computed using the DOE strategy during the optimisation process. The two methods to evaluate the sensitivity are compared in Table 8 and Fig. 11 and also in this case the obtained values are correlated.

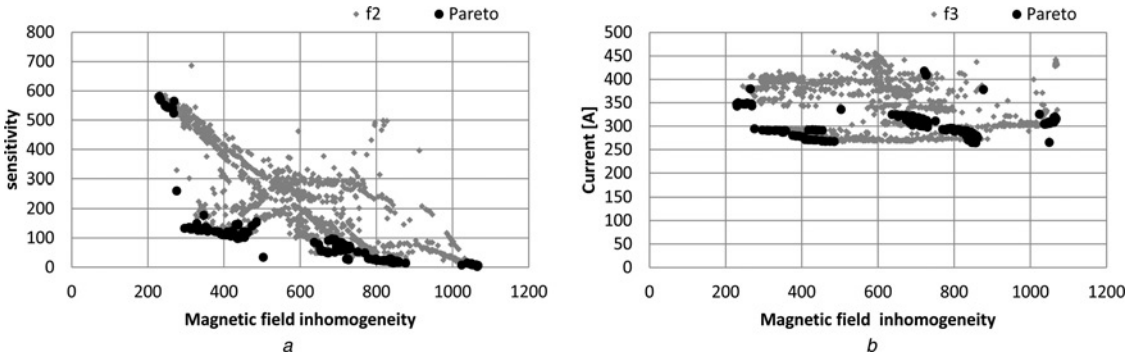

Fig. 8 *2D projections of Pareto front*

a Sensitivity
b Supply current against H inhomogeneity

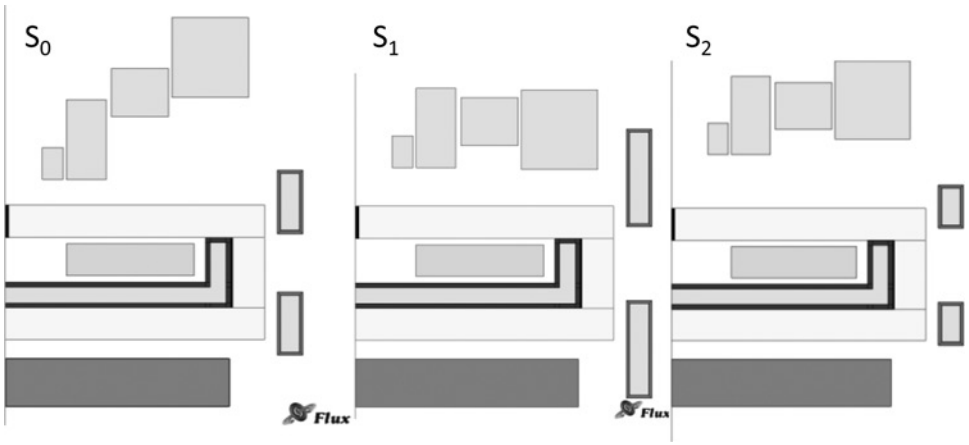

Fig. 9 *Geometries of the designed device for solutions on Pareto front for the case (b)*

IET Sci. Meas. Technol., 2015, Vol. 9, Iss. 5, pp. 579–586

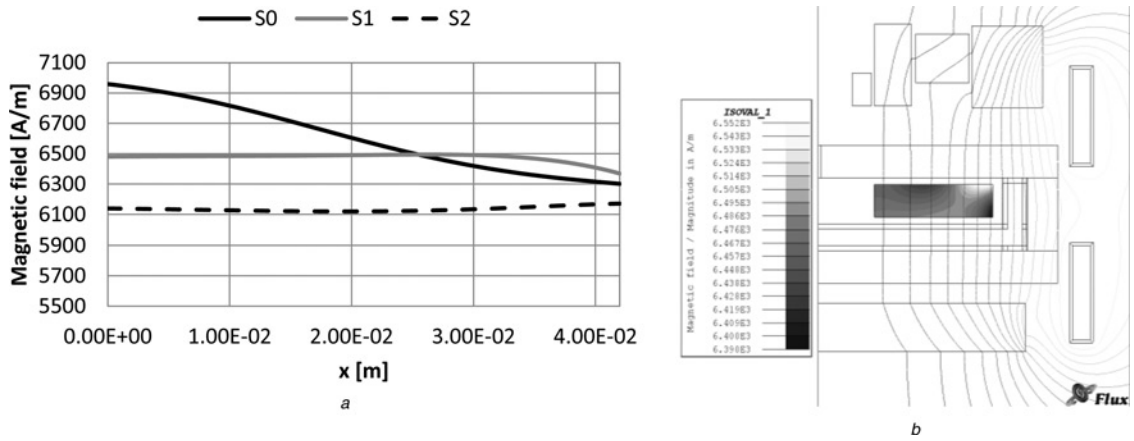

Fig. 10 *Magnetic flux lines and the magnetic field intensity on the Petri dish*

a Magnetic field in the bottom of the Petri dish as a function of the *x*-coordinate
b Magnetic flux line of direct problem and magnetic field colour map on the Petri dish for solution S_1

Table 7 Effect of a variation $d = \pm 1$ mm on the solutions listed in Table 6

		hf_0, mm	hf_1, mm	hf_2, mm	H_s, mm	st, mm	f_1	f_2	f_3, A
S_0	start	1	20.7	26.7	19.8	17.2	1041	13.7	304.2
	round	1	21	27	20	17	1040	13.5	304.8
	$hf_{0,+}$	2	21	27	20	17	1033	16.5	305.3
	$hf_{0,-}$	0	21	27	20	17	1046	10	304.3
	$hf_{1,+}$	1	22	27	20	17	1037	13.7	305.1
	$hf_{1,-}$	1	20	27	20	17	1043	13.6	304.5
	$hf_{2,+}$	1	21	28	20	17	1040	13.7	304.7
	$hf_{2,-}$	1	21	26	20	17	1040	14.2	304.8
S_1	start	5.1	12.1	4.5	30.8	22	228	575.9	346.9
	round	5	12	5	31	22	322	517	348
	$hf_{0,+}$	6	12	5	31	22	524	261.9	348.3
	$hf_{0,-}$	4	12	5	31	22	800	294.9	347.6
	$hf_{1,+}$	5	13	5	31	22	318	531	348
	$hf_{1,-}$	5	11	5	31	22	324	498.3	347.9
	$hf_{2,+}$	5	12	6	31	22	762	314	348.6
	$hf_{2,-}$	5	12	4	31	22	543	258.4	347.4
S_2	start	10.3	18.3	15.2	13.8	22.4	348	126.3	290.3
	round	10	18	15	14	22	397	140.9	290.4
	$hf_{0,+}$	11	18	15	14	22	395	263.2	290.8
	$hf_{0,-}$	9	18	15	14	22	524	174.7	290
	$hf_{1,+}$	10	19	15	14	22	418	145.4	290.5
	$hf_{1,-}$	10	17	15	14	22	362	134.3	290.3
	$hf_{2,+}$	10	18	16	14	22	481	127.8	290.7
	$hf_{2,-}$	10	18	14	14	22	338	196.9	290.1

Table 8 Approximated partial derivatives computed using (6) and sensitivity, for solutions in Table 3, exploiting (5), (7) and Table 7

	$\partial f_1/\partial(hf_0)$	$\partial f_1/\partial(hf_1)$	$\partial f_1/\partial(hf_2)$	$\sigma_{i,\,n}(S_n)$ (7)	f_2 (5)
S_0	−6.5	−3	0	8.3	13
S_1	−138	−3	109.5	203.4	579.3
S_2	−64.5	28	71.5	115.8	122.3

Also for case (b), the lower sensitivity corresponds to the worst case in terms of magnetic field intensity uniformity, whereas it can be observed that considering solution with a better uniformity, the sensitivity increases. Moreover, considering the third objective function, the better solution shows a lower sensitivity.

The proposed multi-objective optimisation gives to the designer the possibility to select the best feasible solutions in terms of field uniformity and in accordance with the power supply characteristics. The designer has to decide to achieve an excellent field uniformity using a weak solution in terms of sensitivity or vice versa accordingly to the his/her experience in practical realising such a kind of devices. For instance, referring to Table 7, the selection of an optimal solution in terms of robustness could be S_0 at the expenses of a higher inhomogeneity; in contrast a solution like S_1 would be oriented to a more uniform magnetic field, but with higher sensitivity to fabrication tolerances. The final choice depends on the quality of the available manufacturing technology.

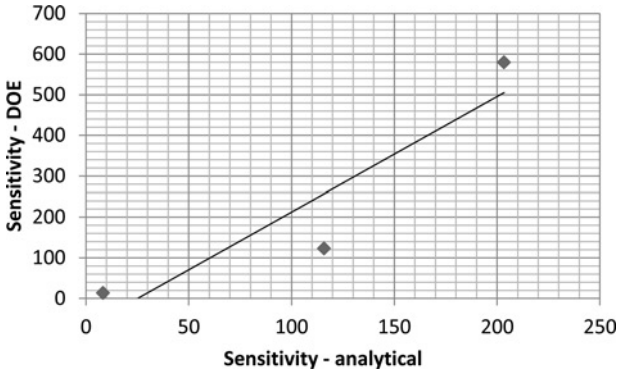

Fig. 11 *Sensitivity – DOE computed using (5) as a function of sensitivity – analytical computed using (7) for the case (b)*

Accordingly to the optimisation results, the Laboratory for the Electroheat of Padua University will realise an inductor with high uniformity of magnetic field, with low supplied voltage and accepting a quite high sensitivity. This design has been realised to carry out laboratory experiments where a high-precision inductor manufacturing is required.

5 Conclusion

Optimisation algorithms coupled to commercially available numerical tools can be used for the robust design of electromagnetic devices. Sensitivity analysis allows evaluating the influence effect of a variation on design variables on an objective function. This is important because during the production process, the device or component is affected by manufacturing tolerances. Sensitivity computation can help the designer to exclude solutions largely affected by tolerance deviations.

Actually, sensitivity is used in manifold ways: for example, it could be evaluated just at the start of the optimisation procedure, by means of a technique of design of computer experiments, in order to identify a reduced set of design variables and so discard the less sensitive ones. Alternatively, it can be evaluated at the end of the optimisation procedure, in order to assess the robustness of the optimised solution; moreover, when sensitivity is incorporated in the objective or constraint functions, there is an extra cost at each iteration for simulating the local perturbation. In this paper, sensitivity has been computed in a cost-effective way exploiting a multi-factorial approach to the DOEs; subsequently, sensitivity has been considered as an auxiliary objective function, in addition to the main design criterion: therefore a multi-objective design problem is originated that has been solved according to Pareto optimality theory; the proposed method has been validated by means of a real-life case study.

6 Acknowledgment

This work is supported by a grant 'Progetto di Ateneo' of the Padua University (CPDA114144).

7 References

1 Ren, Z., Pham, M.-T., Song, M., Kim, D.-H., Koh, C.-s.: 'A robust global optimization algorithm of electromagnetic devices utilizing gradient index and multi-objective optimization method', *IEEE Trans. Magn.*, 2011, **47**, (5), pp. 1254–1257
2 Ren, Z., Pham, M.-T., Koh, C.S.: 'Robust global optimization of electromagnetic devices with uncertain design parameters: comparison of the worst case optimization methods and multiobjective optimization approach using gradient index', *IEEE Trans. Magn.*, 2013, **49**, (2), pp. 851–859
3 Ren, Z., Zhang, D., Koh, C.-S.: 'New reliability-based robust design optimization algorithms for electromagnetic devices utilizing worst case scenario approximation', *IEEE Trans. Magn.*, 2013, **49**, (5), pp. 2137–2140
4 Ren, Z., Park, C., Koh, C.-S.: 'Numerically efficient algorithm for reliability-based robust optimal design of TEAM problem 22', *IEEE Trans. Magn.*, 2014, **50**, (2), pp. 661–664
5 Coenen, I., Gracia, M.H., Hameyer, K.: 'Influence and evaluation of non-ideal manufacturing process on the cogging torque of a permanent magnet excited synchronous machine', *COMPEL – Int. J. Comput. Math. Electr. Electron. Eng.*, 2011, **30**, (3), pp. 876–884
6 Abdallh, A., Crevecoeur, G., Dupré, L.: 'Impact reduction of the uncertain geometrical parameters on magnetic material identification of an EI electromagnetic inductor using an adaptive inverse algorithm', *J. Magn. Magn. Mater.*, 2012, **324**, (7), pp. 1353–1359
7 Alotto, P., Molfino, P., Molinari, G.: 'Optimisation of electromagnetic devices with uncertain parameters and tolerances in the design variables', *COMPEL – Int. J. Comput. Math. Electr. Electron. Eng.*, 2001, **20**, (3), pp. 808–812
8 Aghabeigi, M., Movahhedy, M.R.: 'An algorithm for geometrical uncertainty analysis in planar truss structures', *Struct. Multidiscip. Optim.*, 2014, **49**, (2), pp. 225–238
9 Jayaprakash, G., Thilak, M., SivaKumar, K.: 'Optimal tolerance design for mechanical assembly considering thermal impact', *Int. J. Adv. Manuf. Technol.*, 2014, **73**, pp. 859–873
10 Saravanan, A., Balamurugan, C., Sivakumar, K., Ramabalan, S.: 'Optimal geometric tolerance design framework for rigid parts with assembly function requirements using evolutionary algorithms', *Int. J. Adv. Manuf. Technol.*, 2014, **73**, pp. 1219–1236
11 Lee, S., Kim, K., Cho, S., Jang, J., Lee, T., Hong, J.: 'Optimal design of interior permanent magnet synchronous motor considering the manufacturing tolerances using Taguchi robust design', *IET Electr. Power Appl.*, 2014, **8**, (1), pp. 23–28
12 Pleshivtseva, Y.E., Rapoport, E.Y.: 'The successive parameterization method of control actions in boundary value optimal control problems for distributed parameter systems', *J. Comput. Syst. Sci. Int.*, 2009, **48**, (3), pp. 351–362
13 Hsu, C.-C., Chang, S.-C., Yu, C.-Y.: 'Tolerance design of robust controllers for uncertain interval systems based on evolutionary algorithms', *IET Control Theory Appl.*, 2007, **1**, (1), pp. 244–252
14 Kim, D.-H., Sykulski, J.K., Lowther, D.: 'Design optimisation of electromagnetic devices using continuum design sensitivity analysis combined with commercial EM software', *IET Sci. Meas. Technol.*, 2007, **1**, (1), pp. 30–36
15 Di Barba, P.: 'Multiobjective shape design in electricity and magnetism' (Springer, Doredrecht; New York, 2010)
16 Di Barba, P., Dughiero, F., Sieni, E.: 'Magnetic field synthesis in the design of inductors for magnetic fluid hyperthermia', *IEEE Trans. Magn.*, 2010, **46**, (8), pp. 2931–2934
17 Di Barba, P., Dughiero, F., Forzan, M., Sieni, E.: 'Parametric vs non-parametric optimal design of induction heating devices', *Int. J. Appl. Electromagn. Mech.*, 2014, **44**, (2), pp. 193–199
18 Di Barba, P., Dughiero, F., Sieni, E.: 'Non-parametric optimal shape design of a magnetic device for biomedical applications', *COMPEL – Int. J. Comput. Math. Electr. Electron. Eng.*, 2012, **31**, (5), pp. 1358–1367
19 Di Barba, P., Dughiero, F., Sieni, E.: 'Parameter-free paretian optimisation in electromagnetics: a kinematic formulation', *IET Sci. Meas. Technol..*, 2013, **7**, (2), pp. 93–103
20 Campelo, F., Watanabe, K., Igarashi, H.: 'Topology optimization with smoothness considerations', *Int. J. Appl. Electromagn. Mech.*, 2008, **28**, (1), pp. 187–192
21 Kim, Y.S., Byun, J.K., Park, I.H.: 'A level set method for shape optimization of electromagnetic systems', *IEEE Trans. Magn.*, 2009, **45**, (3), pp. 1466–1469
22 Di Barba, P., Pleshivtseva, Y., Rapoport, E., *et al.*: 'Multi-objective optimisation of induction heating processes: methods of the problem solution and examples based on benchmark model', *Int. J. Microstruct. Mater. Prop.*, 2013, **8**, (4), pp. 357–372
23 Di Barba, P., Dughiero, F., Sieni, E.: 'Synthesizing a nanoparticle distribution in magnetic fluid hyperthermia', *COMPEL – Int. J. Comput. Math. Electr. Electron. Eng.*, 2011, **30**, (5), pp. 1507–1516
24 Di Barba, P., Dughiero, F., Sieni, E.: 'Synthesizing distributions of magnetic nanoparticles for clinical hyperthermia', *IEEE Trans. Magn.*, 2012, **48**, (2), pp. 263–266
25 Di Barba, P., Dughiero, F., Sieni, E.: 'Field synthesis for the optimal treatment planning in magnetic fluid hyperthermia', *Arch. Electr. Eng.*, 2012, **61**, (1), pp. 57–67
26 Alotto, P., Baumgartner, U., Freschi, F., *et al.*: 'SMES optimization benchmark extended: introducing Pareto optimal solutions into TEAM22', *IEEE Trans. Magn.*, 2008, **44**, (6), pp. 1066–1069
27 Fulginei, F., Salvini, A.: 'The flock of starlings optimization: influence of topological rules on the collective behavior of swarm intelligence', in Wiak, S., Napieralska-Juszczak, E.(Eds.): 'Computational methods for the innovative design of electrical devices' (Springer, Berlin, Heidelberg, 2011), pp. 129–145
28 Goya, G.F., Asín, L., Ibarra, M.R.: 'Cell death induced by AC magnetic fields and magnetic nanoparticles: current state and perspectives', *Int. J. Hyperth.*, 2013, **29**, (8), pp. 810–818
29 Hildebrandt, B., Wust, P., Ahlers, O., *et al.*: 'The cellular and molecular basis of hyperthermia', *Crit. Rev. Oncol./Hematol.*, 2002, **43**, (1), pp. 33–56
30 Jordan, A., Scholz, R., Wust, P., Fahling, H., Felix, R.: 'Magnetic fluid hyperthermia (MFH): cancer treatment with AC magnetic field induced excitation of biocompatible superparamagnetic nanoparticles', *J. Magn. Magn. Mater.*, 1999, **201**, (1–3), pp. 413–419
31 Di Barba, P., Dughiero, F., Sieni, E., Candeo, A.: 'Coupled field synthesis in magnetic fluid hyperthermia', *IEEE Trans. Magn.*, 2011, **47**, (5), pp. 914–917
32 Rosensweig, R.E.: 'Heating magnetic fluid with alternating magnetic field', *J. Magn. Magn. Mater.*, 2002, **252**, (1–3), p. 370
33 Fortin, J.P., Gazeau, F., Wilhelm, C.: 'Intracellular heating of living cells through Neel relaxation of magnetic nanoparticles', *Eur. Biophys. J. : EBJ.*, 2008, **37**, (2), pp. 223–228
34 Di Barba, P., Dughiero, F., Forzan, M., Sieni, E.: 'A paretian approach to optimal design with uncertainties: application in induction heating', *IEEE Trans. Magn.*, 2014, **50**, (2), pp. 917–920
35 Plackett, R.L., Burman, J.P.: 'The design of optimum multifactorial experiments', *Biometrika*, 1946, **33**, (4), pp. 305–325
36 13005 E. Guide to the expression of uncertainty in measurement, 1999
37 Bertani, R., Ceretta, F., Di Barba, P., *et al.*: 'Optimal inductor design for nanofluid magnetic characterisation' (Annecy, France, 2014)
38 FLUX. (CEDRAT). Available at http://www.cedrat.com/software/flux/flux.html
39 Binns, K.J., Lawrenson, P.J., Trowbridge, C.W.: 'The analytical and numerical solution of electric and magnetic fields' (Wiley, Chichester, 1992)
40 Deb, K.: 'Multi-objective optimization using evolutionary algorithms' (John Wiley & Sons, Chichester, New York, 2001, 1st edn.)